Nanoscale

Accepted Manuscript

This article can be cited before page numbers have been issued, to do this please use: J. Spitzberg, X. F. van Kooten, M. Bercovici and A. Meller, *Nanoscale*, 2020, DOI: 10.1039/D0NR05000H.

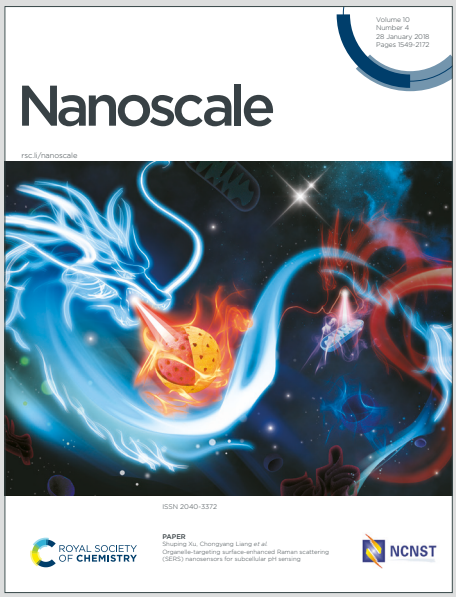

ROYAL SOCIETY OF CHEMISTRY

rsc.li/nanoscale

View Article Online
DOI: 10.1039/D0NR05000H

ARTICLE

Received 00th January 20xx,
Accepted 00th January 20xx

DOI: 10.1039/x0xx00000x

Microfluidic device for coupling isotachophoretic sample focusing with nanopore single-molecule sensing

Joshua D. Spitzberg,[a] Xander F. van Kooten,[a] Moran Bercovici,[a,b] and Amit Meller [a,c,†]

Solid-state nanopores (NPs) are label-free single-molecule sensors, capable of performing highly sensitive assays from a small number of biomolecule translocation events. However, single-molecule sensing is challenging at extremly low analyte concentrations due to the limited flux of analytes to the sensing volume. This leads to a low event rate and increases the overall assay time. In this work, we present a method to enhance the event rate at low analyte concentrations by using isotachophoresis (ITP) to focus and deliver analytes to a nanopore sensor. Central to this method is a device capable of performing ITP focusing directly on a solid-state NP chip, while preventing the focusing electric field from damaging the nanopore membrane. We discuss considerations and trade-offs related to the design of the focusing channel, the ITP electrolyte system and electrical decoupling between the focusing and sensing modes. Finally, we demonstrate an integrated device wherein the concentration enhancement due to ITP focusing leads to an increase in event rate of >300-fold in the ITP-NP device as compared to the NP-only case.

1. Introduction

1.1 Single-molecule nanopore sensing

Single-molecule counting of bioanalytes offers several advantages over ensemble-averaged measurements. For example, measurements of individual molecules can highlight heterogeneity in samples, or identify rare molecules that may be obscured by abundant species in ensemble measurements.

Nanopore (NP) sensors are single-molecule biosensors that electrophoretically characterize analytes by threading them through a molecular-scale aperture. A localized electric field gradient at the pore causes charged analytes to thread and serially translocate from the *cis* to the *trans* side of the aperture. During translocation, the occlusion of the pore causes a current blockade that is characteristic of the biomolecule's shape and charge. If the pore is small enough, single-molecule occupancy is ensured, thereby enabling identification of individual biomolecules.[1] This property has been used for DNA sequencing,[2] protein characterization,[3] pathogen genotyping,[4] and methylation mapping.[5]

Despite its ability to distinguish single molecules, nanopore sensing remains challenging at extremely low concentrations. In the vicinity of a nanopore, electrically charged molecules are actively transported by a strong electric field gradient. However, outside this so-called "capture hemisphere" the delivery of analytes to the nanopore is diffusion-limited (~1-10 s^{-1} nM^{-1} for sub-10 nm pores).[6] As a result, when dealing with extremely low analyte concentrations, the time required to collect a statistically relevant number of translocation events may become prohibitively long for many clinically relevant biomarkers.[7]

Several methods have recently been proposed to improve the effective capture rate, such as different ionic strengths in *cis* and *trans*,[6] plasmon-induced negative thermophoresis of DNA towards the pore,[8] dielectrophoretic trapping of analytes with modified glass nanopipettes,[9] and lipid-anchored ligands that collect analytes *via* specific adsorption, inducing frequent translocation during desorption.[10] In parallel, embedding nanopore biosensors in microfluidic devices has been shown to be a useful approach for manipulation and delivery of small sample volumes before sensing.[11] To simultaneously address both goals of delivery and sample pre-concentration, we couple to the nanopore an electrokinetic technique that directly transports analytes from the sample reservoir, and concentrates them at the sensor for an overall enhanced single-molecule throughput.

1.2 Isotachophoresis

Electrokinetic focusing methods have been used to pre-concentrate analytes prior to downstream analytical processes such as separations[12] and sensing.[13] Isotachophoresis (ITP) is a particularly powerful electrokinetic technique that selectively focuses analytes into a concentrated zone at a moving interface between two ionic species with different electrophoretic mobilities.[14] ITP has been used to focus

[a.] Department of Biomedical Engineering, The Technion – Israel Institute of Technology, Haifa, 32000 Israel.
[b.] Department of Mechanical Engineering, The Technion – Israel Institute of Technology, Haifa, 32000 Israel.
[c.] Department of Biomedical Engineering, Boston University, Boston, MA 02215 USA
† Email: ameller@technion.ac.il.

Electronic Supplementary Information (ESI) available: Co-focusing of tracking dye and labeled DNA; ITP calibration factor; pore diameter calculation;event diagram; event-rate scaling,. See DOI: 10.1039/x0xx00000x

View Article Online
DOI: 10.1039/D0NR05000H

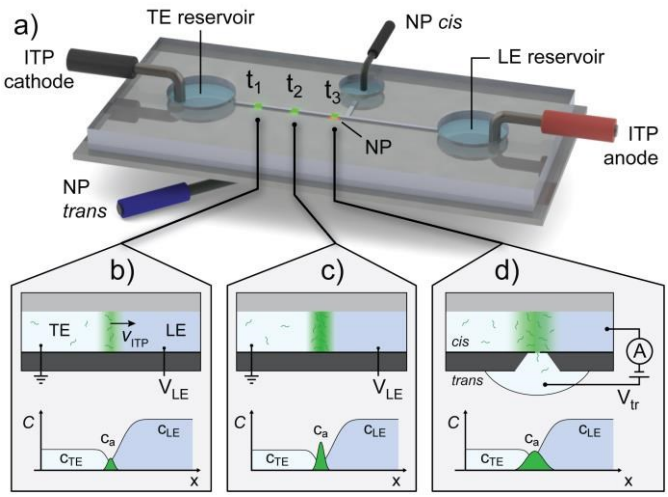

Figure 1. Concept of ITP-NP sensing. **(a)** Focusing and delivery of analytes to a solid-state nanopore (NP) using isotachophoresis. **(b)** Schematic cross-section and concentration profiles along the microchannel. The analytes (shown in green) are initially mixed with TE in the left reservoir. When V_{LE} is applied between the ITP anode and cathode, analytes focus at the interface between a low-mobility TE and high-mobility LE. **(c)** The analyte concentration increases as the interface migrates downstream. **(d)** When the focused zone reaches the nanopore, the focusing voltage is removed and a translocation bias is applied across the membrane (*cis* to *trans*). The locally enhanced analyte concentration due to ITP focusing leads to an increased translocation event rate.

nucleic acids[15] and proteins[16] from biological matrices such as whole blood,[17,18] serum[16] and urine[19], and can yield concentration enhancements of up to five orders of magnitude using biologically compatible buffer systems.[20] The extreme focusing capability of ITP has been leveraged to enhance binding kinetics in homogeneous[19,21] and surface-based[22–24] assays, leading to a remarkable increase in sensitivity.

In this work we demonstrate for the first time the integration of ITP focusing with single-molecule NP sensing. This method relies on a custom device that enables precise delivery of the focused ITP zone to a nanopore sensor, while preventing the focusing electric field gradient from damaging the nanopore. We discuss considerations in the design of the device related to rapid switching between focusing and sensing, and show that ITP focusing in such a device enables an improvement in the capture rate by over two orders of magnitude.

2. Results and discussion

2.1 ITP-enhanced nanopore sensing

The concept of ITP-NP sensing is shown schematically in Figure 1. ITP uses a discontinuous buffer system consisting of a terminating (TE) and leading electrolyte (LE), which contain ions with an electrophoretic mobility that is respectively lower and higher than that of the analyte of interest. The ITP channel and one reservoir are initially filled uniformly with LE, and a mixture of TE and analytes is placed in the other reservoir (Figure 1a). When a voltage is applied between the TE and LE reservoir, analytes focus at the moving interface between the TE and LE (Figure 1b). Accumulation of analyte continues while the focused zone electromigrates along the channel (Figure 1c).

Once the interface reaches the nanopore, the focusing field is removed and a low-voltage bias is applied between the *cis* and *trans* reservoirs (V_{tr}) on either side of the nanopore, causing the analyte to translocate through the pore (Fig. 1d). The increased concentration in the vicinity of the pore due to ITP focusing leads to a higher event rate and rapid sensing at lower analyte concentrations.

2.2 Design and assembly of the ITP-NP device

Effective coupling of ITP focusing and nanopore sensing requires delivery of a focused zone directly to the NP with minimal loss of concentration. To achieve this, we used a solid-state nanopore chip as a substrate for a microchannel in which we focused analytes using ITP. We developed and fabricated a custom ITP-NP device that facilitated the alignment and bonding of the microchannel to the NP chip, as well as subsequent steps related to the formation and use of the nanopore sensor.

Figure 2a shows an expanded schematic view of the ITP-NP device. The Teflon base of the device provides electrical and fluidic access to the *trans* side of the nanopore. The nanopore chip containing the NP membrane acts as a substrate for the microfluidic layer, which contains the ITP focusing channel and provides access to the *cis* side of the NP. Fluidic and electrical access was provided through a frame that held the focusing and sensing electrodes, with a cut-out to allow visualization of the channel (Figure 2b). We aligned the PDMS microchannel to the free-standing SiN_x membrane using a micropositioner, so that the membrane was located exactly 10 mm into the channel. The channel was then clamped with magnets. A glass slide distributed pressure to avoid deforming the PDMS. The device was enclosed in a

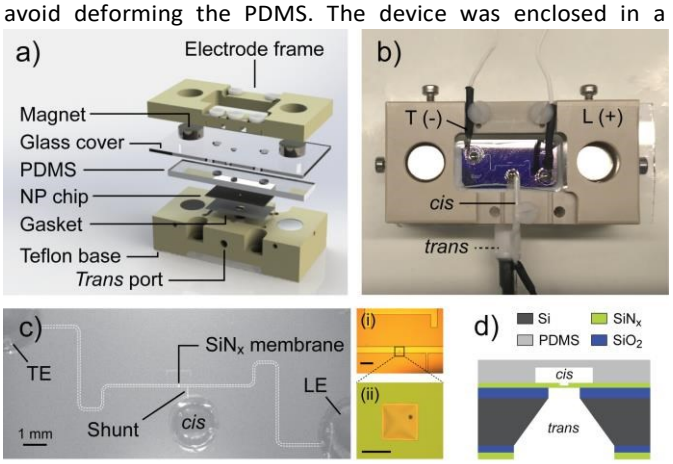

Figure 2. Design, fabrication and assembly of the ITP-NP device. **(a)** Expanded schematic view of the device. The Teflon base provides fluidic and electrical access to the *trans* side of the pore. The solid-state NP chip supports a PDMS microfluidic layer, in which ITP focusing takes place. The channel is sealed and held in place with magnets. **(b)** Top view of an assembled device, showing the platinum ITP cathode and anode (T and L, respectively) and the Ag/AgCl *cis* and *trans* electrodes. The length of the electrode frame is 5 cm. **(c)** Top view of the ITP focusing channel and nanopore as seen through an upright microscope. Panels (i) and (ii) show an enlarged view of the membrane in the focusing channel (scale bars denote 200 µm and 20 µm, respectively). The thin region, in which a nanopore is formed by dielectric breakdown, is visible as a dark dot in panel (ii). **(d)** Schematic cross-section of a nanopore chip sealed against a PDMS microchannel (not to scale).

Faraday cage to shield it from ambient electrical noise.

The design of the microchannel (Figures 2c) offers a compromise between a high ITP concentration factor and a short focusing time (~3 min). The channel has a uniform width of 100 µm, a depth of 35 µm and a length of 20 mm. (Figure 2d). The nanopore was drilled in a thinned region of the membrane using controlled dielectric breakdown after assembling the device. A more detailed description of the assembly can be found in Materials and Methods.

2.3 Electrical Decoupling

Initial experiments, in which a high voltage was applied to the focusing channel running along the *cis* side of the nanopore membrane, resulted in mechanical deformation of the thin membrane and expansion of the nanopore, presumably due to electromechanical stress exerted on the dielectric membrane. However, we found that the pore remained intact if the voltage ramp was limited to 20 Vs^{-1}, and if the *cis* and *trans* sides were held at the same potential during ITP. To achieve this, we added a side channel immediately downstream of the nanopore that was electrically connected on its other end to the *trans* side of the nanopore. The channel was filled with LE electrolyte and provided a low-resistance path, or 'shunt' between the two sides of the pore. Fig. 3 presents the electrical schematic of the system. In *ITP mode*, a high voltage is applied across the focusing channel and the shunt connection is closed (relays S1, S2 and S3 closed, S4 open). In *NP mode*, the high voltage source is disconnected (relays S1 and S2 open), the shunt is disconnected (S3 open) and a translocation bias is applied across the nanopore (S4 closed).

We used a set of low-noise, fast-switching optical relays to perform the decoupling of the two modes, as we found that these reduced the injection of electrical noise from the high-voltage ITP power supply into the sensitive translocation high-gain pre-amplifier ('headstage') that monitors NP current. With the relays in place, the electrical RMS noise measured at 100 KHz bandwidth was <150 pA, compared to an open-pore current of >3 nA. The relays were operated by custom LabVIEW control software, allowing very rapid transition between the modes such that the first translocations are detected almost immediately after arrival of the ITP zone, when the concentration of analyte is the highest.

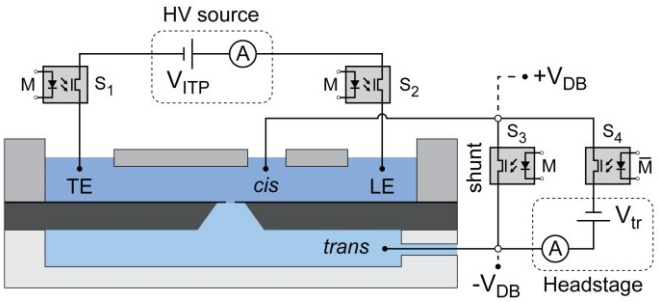

Figure 3. Electrical decoupling of ITP focusing and NP sensing using solid-state relays switched by a control signal (M). During ITP focusing ($M = 1$) the TE and LE electrodes are connected, and the shunt connection from *cis* to *trans* is in place. During NP sensing ($M = 0$) the NP sensing headstage is connected between *cis* and *trans*, while the high-voltage ITP source is isolated from the system. This configuration enables ITP focusing without causing damage to the dielectric membrane or expanding the nanopore, and substantially reduces injection of electrical noise into the sensing headstage. The voltage V_{DB} is only applied during *in-situ* formation of a nanopore using controlled dielectric breakdown.

2.4 ITP Focusing

Since the ITP buffer system also serves as the *cis* electrolyte for the NP, the system should be optimized to account for both. Translocation of DNA is typically performed under a high KCl concentration on the *cis* side, between 500-1,000 mM. Although the ITP focusing rate improves as the LE to TE conductivity ratio increases, a very high ionic strength LE reduces the effective mobilities,[25] primarily of multivalent species, degrading the focusing ability.[26] Furthermore, since DNA focuses at the interface between the LE and TE, the *cis* electrolyte is in practice a mixture of the two buffers. We found that an LE composed of 600 mM KCl, 175 mM HCl, 200 mM tris, and a TE composed of 20 mM tris and 10 mM tricine provided both adequate translocation and focusing. Figure 4 presents the characterization of DNA focusing under these conditions in a PDMS/SiN_x microchannel with the same geometry and depth as the channel used in the ITP-NP device. The analyte was 10 pM dsDNA (1994 bp), covalently labelled with ATTO 550 fluorescent dye (see *Materials and Methods*) and mixed with the TE. Figure 4a shows the electromigration of the focused ITP zone in the channel at regular intervals. The inset shows a microscope image of the focused zone, with a length of ~80 µm at the location of the NP membrane. A video showing the focusing process from the sample reservoir to the NP membrane is included in the SI.

The amount of analyte accumulated after a distance x along the channel is given by $N_A = \eta c_i A x$, and the characteristic concentration in the focused zone is $c_i^{ITP} = N_A / A\delta = \eta c_i^0 x$, where A is the channel cross-section, δ is the width of the focused zone, c_i^0 is the initial concentration of the analyte, and η is dependent on the ionic properties of the system.[26] For low analyte concentrations (relative to those of the LE or TE), the focusing ratio ($c_i^{ITP}/c_i^0 = \eta x$) is independent of the initial analyte concentration in the reservoir. Figure 4b shows the integrated fluorescence intensity of the zone during electromigration, which is a measure for the accumulated analyte mass, and is in agreement with theory. The mean concentration of the delivered ITP zone was determined by averaging the fluorescence intensity over a region of interest, and the corresponding concentration was calculated using a fluorescence calibration curve (see SI). The mean zone concentration at the location of the nanopore was 1.15 ± 0.33 nM (n=3), corresponding to a focusing factor of 1150 ± 330.

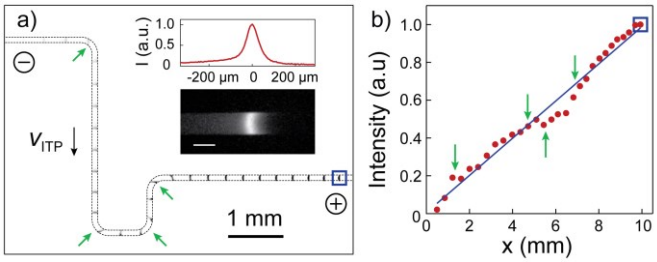

Figure 4. Experimental characterization of ITP focusing. **(a)** Overlaid fluorescence microscopy images showing the ITP zone at 5 s intervals. The microchannel is indicated with dashed lines. The TE reservoir at the cathode side contains 10 pM dsDNA (1994 bp) labeled with ATTO 550. The inset shows a fluorescence image of the focused ITP zone and the axial intensity profile along the channel, used to quantify the focusing (scale bar is 100 µm). **(b)** The integrated fluorescence intensity, which is a measure for the total mass of analyte in the ITP zone, follows the expected linear increase over the length of the channel. Green arrows indicate the location of turns in the channel, and the blue square indicates the location of the nanopore, as shown in (a).

2.5 ITP-Nanopore sensing

To quantify the performance of the ITP-NP device, we performed NP sensing with and without ITP focusing. For NP-only sensing, we used a NP chip without a PDMS microchannel, and filled the *trans* reservoir with LE buffer (see *Materials and Methods*). On the *cis* side, we placed a droplet of LE buffer containing 1 nM dsDNA (5054 bp). The pore diameter was estimated at 5.4 nm, based on an open-pore current of 5.7 nA, a buffer conductivity of 7.6 S m^{-1}, and 500 mV bias (see SI). For ITP-NP sensing, we co-focused in the channel (*cis* side of the chip) 1 pM of the same dsDNA (5054 bp) and 100 pM of Dylight 488. We visually tracked the location of the focused zone and switched to NP sensing once it reached the nanopore. Here, the pore diameter was estimated at 6.4 nm, based on an open-pore current of 6.2 nA, a buffer conductivity of 6.2 S m^{-1}, and 500 mV bias.

Figure 5 shows representative translocation events as a series of individually concatenated ionic current traces for NP-only (Fig. 5a) and ITP-NP experiments (Fig. 5b. Histograms of the dwell time (t_D) and fractional current blockade - the ratio of blocked pore current amplitude to open-pore current amplitude ($IB = i_B/i_O$) - are presented in the middle and right-hand panels, respectively. In both cases we used double Gaussian functions to fit the normalized current blockade histogram, reflecting the possibility of linear and folded DNA translocations. The hyperbolic profile of the event diagram for the NP-only experiment indicates a mixed population of events (see SI-4). As expected, the smaller nanopore (Fig. 5a) showed slightly longer dwell times and deeper events (lower values of I_B).[26,27] The mean dwell time is obtained from an exponential fit of the blockade histograms, as indicated.

Figure 5c shows the histogram of the time between translocation events. The capture rate of analytes can be characterized by exponential fits to the inter-event time (δt). We obtained a NP-only event rate of 5.43 ±0.03 s^{-1} and an ITP-NP event rate of 2.56 ± 0.11 s^{-1}. However, we note that the initial concentration in ITP-NP sensing was three orders of magnitude lower than for the NP-only case. This difference is

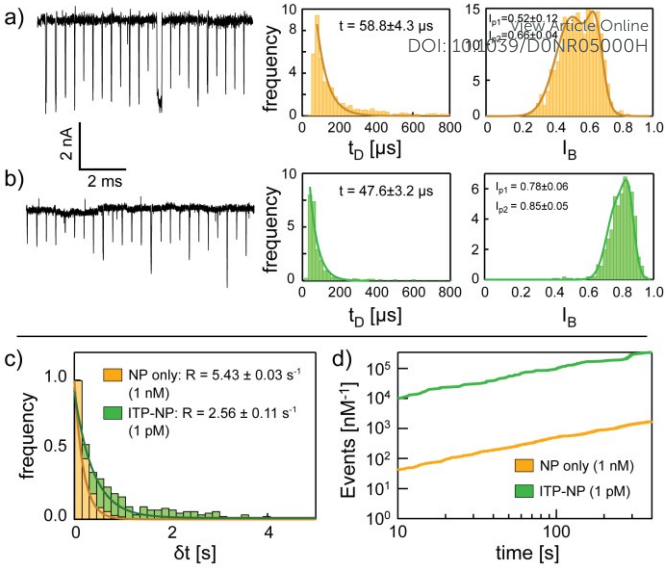

Figure 5. Experimental comparison of NP sensing with and without ITP focusing. **(a)** NP measurements without ITP focusing. The analyte is 1 nM dsDNA (5054 bp). Left panel: concatenated ionic current trace of translocation events. Center panel: histogram of the dwell time (t_D) with an exponential fit indicating a mean expected duration. Right panel: Histogram of the relative blockade depth (I_B). The double-Gaussian fit indicates a mixture of linear (shallow) and folded (deep) translocations. **(b)** NP measurements with ITP focusing. The analyte is 1 pM dsDNA (5054 bp), with 100 pM Dylight 488 as a co-focusing tracer. **(c)** Histogram of the time between translocation events. The event rate is similar for NP-only and ITP-NP (5.43 s^{-1} and 2.56 s^{-1}, respectively), despite a 1000-fold lower initial concentration in the latter. **(d)** Cumulative events over time, normalized to the initial concentration in the reservoir (1 nM and 1 pM for the NP-only and NP-ITP case, respectively). This result shows over 2 orders of magnitude enhancement in event rate in the ITP-NP device.

highlighted in Figure 5d, which shows the event rate per nanomolar of initial concentration. These results show a 470-fold increase in event rate for ITP-NP as compared to NP-only sensing. Scaling for differences in pore size results in ~337-fold enhancement of the event rate due to ITP focusing. We believe this rate enhancement is lower than the concentration enhancement of ITP, due to the voltage ramp-down of ITP prior to NP sensing (the zone width is proportional to V_{ITP}), and due to diffusion of the ITP zone during NP sensing.

Conclusions

We have demonstrated and evaluated the use of isotachophoresis to focus and deliver DNA molecules to a nanopore sensor. This was done using a custom device that enabled microfluidic ITP focusing directly on a solid-state nanopore chip.

Central to the ITP-NP device was the ability to decouple the high electric field used for ITP, from the nanopore in the fragile dielectric membrane. Crucially, we found that a limited ITP voltage ramp and a shunt connection from *cis* to *trans* could protect the dielectric membrane from damage resulting from electromechanical stress under high voltage. We implemented a switching circuit using opto-electrical relays, to decouple and rapidly switch between ITP focusing and NP sensing modes, while substantially reducing the injection of noise by the ITP electronics into the NP pre-amplifier.

ITP focusing in a 2 cm channel yielded a 1150-fold concentration enhancement relative to the initial

View Article Online
DOI: 10.1039/D0NR05000H

concentration in the reservoir in approximately 3 min. Delivering a focused ITP zone to the NP led to a >300 increase in translocation event rate as compared to the NP-only case, after correcting for differences in experimental conditions. This enabled detection of dsDNA at 1 pM initial concentration with an event rate of ~2.56 s^{-1}, substantially higher than can be achieved with conventional NP sensing.

A further increase in event rate may be obtained by using longer microchannels or ones with a narrowing geometry, to increase the ITP focusing factor.[20] ITP-NP devices are expected to readily demonstrate further event-rate enhancement if *cis-trans* buffer gradients are used.[6] Moreover, we expect that the ITP-NP method and device demonstrated here are not limited to focusing DNA, but that other analytes can be focused and sensed with an appropriate buffer system. Overall, we believe that the method and device shown here can enhance detection rates by several orders of magnitude, paving the way to rapid single-molecule sensing at low concentrations.

Materials and Methods

Device fabrication and assembly

The microfluidic channel consisted of a primary focusing channel with a length of 20 mm and a width of 100 µm between LE and TE reservoirs joined by a shunt channel 400 µm downstream of the NP membrane. The shunt channel had a length of 1 mm and a width of 50 µm. The height of the channels was 35 µm as defined by the photoresist master.

The photoresist master used to cast the PDMS microfluidic layer was fabricated using soft lithography. The microchannel mold was formed by patterning SU-8 3050 photoresist (MicroChem) on a silicon wafer (University Wafer). After developing the photoresist, the wafer was vapor-coated with trichloro(octyl)silane (Sigma Aldrich), and then covered with polydimethylsiloxane (Sylgard 184, Dow Corning) in a 10:1 ratio of base to crosslinking agent. After curing for 2 hours at 80°C, the microfluidic layer was peeled off the wafer and holes where punched for the cathode (3 mm), anode (3 mm), and shunt (2 mm) reservoirs.

The nanopore chip consisted of a 1x2 cm^2 Si substrate with a freestanding SiN_x membrane. Devices were fabricated from a 4" double-side polished Si wafer coated on both sides with 500 nm SiO_2 and 50 nm low-stress SiN_x. Square windows were patterned on the back side of the wafer by photolithography, and etched through the SiN_x and SiO_2 layers using CF_4/O_2 reactive ion etching (RIE) and buffered oxide etch (BOE), respectively. Next, circular regions 2 µm in diameter were patterned on the front side of the wafer, aligned to the center of the squares on the back side. The SiN_x in these circular regions was etched down to a thickness of 10-15 nm using CF_4/O_2 RIE. Free-standing SiO_2/SiN_x membranes were then formed by wet etching of Si in KOH (33%) at 65 °C. Finally, the SiN_x membranes were released by etching the remaining SiO_2 using BOE. The thickness of the free-standing membranes was 11 nm, as measured by ellipsometry (FS1, FilmSense).

Nanopore chips were cleaned in piranha (H_2SO_4:H_2O_2 3:1) at 100 °C for 10 min, thoroughly rinsed in deionized water, dried with N_2, and mounted on a PDMS gasket (spin-coated and cut to size) which was placed on the opening of the *trans* reservoir (filled with translocation buffer) in the Teflon base. The PDMS channel was made hydrophilic using O_2 plasma to facilitate wetting. The channel was cleaned with ethanol, dried with N_2, and reversibly bonded to the glass cover. The glass cover and PDMS channel were aligned to the freestanding membrane using a 3-axis micropositioner and lowered into contact with the NP chip while observing the alignment through an upright microscope. The device was then mechanically clamped together using 2 pairs of magnets. The microchannel was filled uniformly with LE buffer using vacuum. The Ag/AgCl NP *cis* electrode and the Pt electrodes for ITP were mounted to the electrode frame and inserted into the top-side reservoirs. The Ag/AgCl *trans* electrode was placed into the *trans* reservoir in the Teflon base, and a NP was formed in the dielectric membrane by controlled breakdown of dielectric (CBD) at 0.3 V/nm until a stable pore was formed.[28]

Electrical decoupling and software

Optical solid-state relays (AQW210HL, Panasonic) were used to switch between ITP and NP modes. We used custom LabVIEW software to control and synchronize switching and data collection. A detailed overview of the system diagram is provided in the SI.

Buffers

LE buffer was prepared as 600 mM KCl, 200 mM tris, 175 mM HCl, 1% w/v 1.3 MDa poly-vinylpyrrolidone (PVP). TE buffer contained 20 mM tris and 10 mM tricine. Buffers were filtered with 0.02 µm membranes and degassed prior to use. The co-focusing dye was Dylight-488 free acid (Thermo Fisher Scientific); all other reagents were purchased from Sigma Aldrich.

ITP focusing

The reservoirs and channel were rinsed with deionized water and filled uniformly with LE. We then rinsed the TE reservoir with TE to remove residues of LE, immediately replaced it with TE containing analyte, and applied a 100 V ITP bias voltage using a high voltage source-meter (2410, Keithley Instruments). We tracked the ITP zone by observing the location of the co-focusing fluorescent dye, as detailed below. When the ITP interface reached the nanopore membrane, we removed the ITP voltage. Manually ramping down the voltage from enabled accurate positioning of the ITP zone over the NP.

NP sensing

The system was switched to NP mode. We applied a trans-membrane bias and measured the current using a high-gain pre-amplifier headstage (EPC 9, HEKA Elektronik). The

View Article Online
DOI: 10.1039/D0NR05000H

electrical current through the nanopore was collected using A/D data acquisition boards (6501 and 6211, National Instruments) at 100 kHz sampling rate and low-pass filtered at 30 KHz bandwidth. All experiments were performed with the device enclosed by a copper Faraday cage.

Sample preparation

A 5456 bp DNA fragment was amplified from a pET28b plasmid using PCR. The DNA was separated on 0.7% agarose TAE gel, excised and extracted from the gel using a PCR cleanup kit (Promega).

A 1994 bp DNA fragment was amplified from a 5000 bp NoLimits DNA (Thermo Fisher Scientific) using PCR. The 1994 bps DNA fragment was purified using the PCR cleanup kit (Macherey-Nagel), and labelled using Nick Translation with Aminoallyl-dUTP-ATTO550 (Sigma Aldrich). Finally, the fluorescently dye-labelled sample was purified by QIAQuick PCR cleanup kit (Qiagen)

The final concentrations of both fragments were verified via UV-Vis absorption spectroscopy. The DNA was further purified via ethanol precipitation, aliquoted at 0.1 pmol per tube, dried using a SpeedVac, and subsequently stored at −20 °C. Prior to use, aliquots were rehydrated in 50 microliter MilliQ water to incubated at 70 °C for 15 minutes at 300 rpm, and then serially diluted into the appropriate buffer at desired final concentration.

Fluorescence imaging

We performed all imaging with the ITP-NP device mounted on the stage of an upright microscope (AZ100, Nikon) equipped with 2x and 5x objectives (NA 0.5 AZ Plan Fluor and NA 0.2 AZ Fluor, respectively; Nikon) set to 1x optical zoom, an LED light source (Sola, Lumencor) and a CMOS camera (Zyla 4.2, Andor). We used a FITC filter for detecting the Dylight-488 cofocusing dye, and a TRITC filter for detecting the ATTO-550 labelled DNA.

Data analysis and statistics

Raw intensity values of the ITP zone were corrected for background intensity by imaging the channel filled with water. The zone's mean fluorescence at the location of the membrane was measured by averaging intensity values across all pixels within a region of interest 100 µm wide and 50 µm centered on the zone. An intensity-to-concentration calibration curve was created by filling the channel with known dye concentrations (0.1, 0.25, 0.5, 1.0 µM) and performing a linear fit.

Nanopore events were measured as fractional current blockade, the ratio of blocked pore current amplitude to open-pore current amplitude ($I_B = i_B/i_O$). An event was defined by a drop of 15% below the open pore level, lasting at least 30 µs before spontaneously returning to the open pore level. The time between the starting and ending points was defined as the translocation dwell time (t_D). The average event amplitude is the all-point average during the dwell time. The normalized dwell time histograms were characterized by tail-fitting the data using exponential functions to reduce the effect of extremely fast events limited by the temporal bandwidth of our system. The normalized inter-events time (δt) histograms were fit with an exponential curve to estimate event rates. The event extraction and analysis were done in MATLAB (MathWorks) and Igor Pro (Wavemetrics), respectively.

Conflicts of interest

There are no conflicts to declare.

Acknowledgements

We are grateful to A. Zrehen for developing the control software. This project has received funding from the European Research Council (ERC) under the European Union's Horizon 2020 research and innovation program (grant agreement No. 833399).

References

1 D. Deamer, M. Akeson and D. Branton, *Nat. Biotechnol.*, 2016, **34**, 518–524.

2 E. A. Manrao, I. M. Derrington, A. H. Laszlo, K. W. Langford, M. K. Hopper, N. Gillgren, M. Pavlenok, M. Niederweis and J. H. Gundlach, *Nat. Biotechnol.*, 2012, **30**, 349–353.

3 E. Kennedy, Z. Dong, C. Tennant and G. Timp, *Nat. Nanotechnol.*, 2016, **11**, 968–976.

4 A. H. Squires, E. Atas and A. Meller, *PLoS One*, 2015, **10**, e0142944.

5 A. C. Rand, M. Jain, J. M. Eizenga, A. Musselman-Brown, H. E. Olsen, M. Akeson and B. Paten, *Nat. Methods*, 2017, **14**, 411–413.

6 M. Wanunu, W. Morrison, Y. Rabin, A. Y. Grosberg and A. Meller, *Nat. Nanotechnol.*, 2010, **5**, 160–165.

7 S. O. Kelley, *ACS Sensors*, 2017, **2**, 193–197.

8 F. Nicoli, D. V Verschueren, M. Klein, C. Dekker and M. P. Jonsson, *Nano Lett.*, 2014, **14**, 6917–25.

9 K. J. Freedman, L. M. Otto, A. P. Ivanov, A. Barik, S. Oh and J. B. Edel, *Nat. Commun.*, 2016, **7**, 1–9.

10 E. C. Yusko, J. M. Johnson, S. Majd, P. Prangkio, R. C. Rollings, J. Li, J. Yang and M. Mayer, *Nat. Nanotechnol.*, 2011, **6**, 253–260.

11 N. Varongchayakul, J. S. Hersey, A. Squires, A. Meller and M. W. Grinstaff, *Adv. Funct. Mater.*, 2018, **28**, 1804182.

12 D. M. Osbourn, D. J. Weiss and C. E. Lunte, *Electrophoresis*, 2000, **21**, 2768–2779.

13 C. Eid and J. G. Santiago, *Lab Chip*, 2018, **18**, 11–26.

14 T. P. E. M. V. F.M. Everaerts, J.L. Beckers, *Isotachophoresis:*

View Article Online
DOI: 10.1039/D0NR05000H

Theory, Instrumentation and Applications, Elsevier, Amsterdam, 2011.

15 A. Rogacs, L. A. Marshall and J. G. Santiago, *J. Chromatogr. A*, 2014, **1335**, 105–120.

16 Y. Qu, L. A. Marshall and J. G. Santiago, *Anal. Chem.*, 2014, **86**, 7264–7268.

17 A. Persat, L. A. Marshall and J. G. Santiago, *Anal. Chem.*, 2009, **81**, 9507–9511.

18 L. A. Marshall, C. M. Han and J. G. Santiago, *Anal. Chem.*, 2011, **83**, 9715–9718.

19 M. Bercovici, G. V Kaigala, K. E. Mach, C. M. Han, J. C. Liao and J. G. Santiago, *Anal. Chem.*, 2011, **83**, 4110–4117.

20 X. F. van Kooten, M. Truman-Rosentsvit, G. V Kaigala and M. Bercovici, *Sci. Rep.*, 2017, **7**, 10467.

21 M. Bercovici, C. M. Han, J. C. Liao and J. G. Santiago, *Proc. Natl. Acad. Sci.*, 2012, **109**, 11127–11132.

22 F. Paratore, T. Zeidman Kalman, T. Rosenfeld, G. V Kaigala and M. Bercovici, *Anal. Chem.*, 2017, **89**, 7373–7381.

23 C. M. Han, E. Katilius and J. G. Santiago, *Lab Chip*, 2014, **14**, 2958–2967.

24 A. T. Bender, M. D. Borysiak, A. M. Levenson, L. Lillis, D. S. Boyle and J. D. Posner, *Anal. Chem.*, 2018, **90**, 7221–7229.

25 A. Persat, M. E. Suss and J. G. Santiago, *Lab Chip*, 2009, **9**, 2454–69.

26 T. K. Khurana and J. G. Santiago, *Anal. Chem.*, 2008, **80**, 6300–6307.

27 M. Wanunu, J. Sutin, B. McNally, A. Chow and A. Meller, *Biophys. J.*, 2008, **95**, 4716–25.

28 D. Fologea, M. Gershow, B. Ledden, D. S. McNabb, J. A. Golovchenko and J. Li, *Nano Lett.*, 2005, **5**, 1905–1909.